THE JOURNAL OF BIOLOGICAL CHEMISTRY VOL. 288, NO. 12, pp. 8445–8455, March 22, 2013
Published in the U.S.A.

Conserved Structural Chemistry for Incision Activity in Structurally Non-homologous Apurinic/Apyrimidinic Endonuclease APE1 and Endonuclease IV DNA Repair Enzymes*[S]

Received for publication, October 23, 2012, and in revised form, December 22, 2012 Published, JBC Papers in Press, January 25, 2013, DOI 10.1074/jbc.M112.422774

Susan E. Tsutakawa[‡], David S. Shin[§], Clifford D. Mol[§], Tadahide Izumi[¶‖], Andrew S. Arvai[§], Anil K. Mantha[‖1], Bartosz Szczesny[‖], Ivaylo N. Ivanov[**], David J. Hosfield[§], Buddhadev Maiti[**], Mike E. Pique[§], Kenneth A. Frankel[‡], Kenichi Hitomi[‡§‡‡2], Richard P. Cunningham[§§], Sankar Mitra[‖], and John A. Tainer[‡§3]

From the [‡]Lawrence Berkeley National Laboratory, Berkeley, California 94720, the [§]Scripps Research Institute, La Jolla, California 92037, the [¶]University of Kentucky, Lexington, Kentucky 40536, the [‖]University of Texas Medical Branch, Galveston, Texas 77555, [**]Georgia State University, Atlanta, Georgia 30302, the [‡‡]Graduate School of Engineering Science, Osaka University, Toyonaka, Osaka 560-8531, Japan, and the [§§]University of Albany, State University of New York, Albany, New York 12222

Background: DNA apurinic/apyrimidinic (AP) sites are toxic and mutagenic if unrepaired by AP endonucleases.
Results: Structural, mutational, and computational analyses of prototypic AP endonucleases APE1 and Nfo identify surprising similarities.
Conclusion: APE1 and Nfo reveal functional equivalences illuminating their catalytic reaction.
Significance: A conserved catalytic geometry is specific to AP site removal despite different enzyme structures and metal ions.

Non-coding apurinic/apyrimidinic (AP) sites in DNA form spontaneously and as DNA base excision repair intermediates are the most common toxic and mutagenic *in vivo* DNA lesion. For repair, AP sites must be processed by 5′ AP endonucleases in initial stages of base repair. Human APE1 and bacterial Nfo represent the two conserved 5′ AP endonuclease families in the biosphere; they both recognize AP sites and incise the phosphodiester backbone 5′ to the lesion, yet they lack similar structures and metal ion requirements. Here, we determined and analyzed crystal structures of a 2.4 Å resolution APE1-DNA product complex with Mg^{2+} and a 0.92 Å Nfo with three metal ions. Structural and biochemical comparisons of these two evolutionarily distinct enzymes characterize key APE1 catalytic residues that are potentially functionally similar to Nfo active site components, as further tested and supported by computational analyses. We observe a magnesium-water cluster in the APE1 active site, with only Glu-96 forming the direct protein coordination to the Mg^{2+}. Despite differences in structure and metal requirements of APE1 and Nfo, comparison of their active site structures surprisingly reveals strong geometric conservation of the catalytic reaction, with APE1 catalytic side chains positioned analogously to Nfo metal positions, suggesting surprising functional equivalence between Nfo metal ions and APE1 residues. The finding that APE1 residues are positioned to substitute for Nfo metal ions is supported by the impact of mutations on activity. Collectively, the results illuminate the activities of residues, metal ions, and active site features for abasic site endonucleases.

Apurinic/apyrimidinic (AP)[4] sites are the most common DNA lesions *in vivo*, calculated to be generated at ~10,000 lesions/cell/day in humans (1–3). AP sites form spontaneously or as central DNA repair intermediates during base excision repair (BER) (4). AP sites can block replication and cause mutations, so its repair is critical for genetic integrity (5, 6). Repair of AP sites is carried out via the BER pathway, which creates AP sites by uracil and alkylated base-specific monofunctional DNA glycosylases that excise the base lesion to produce AP sites (7). For the glycosylases, structures were key to revealing that specificity is encoded in nucleotide flipping and binding, as shown by MutY and uracil-DNA glycosylase (8, 9). The AP sites produced by excision of the damaged base are the substrates of AP endonucleases. For AP endonucleases, there are primarily two distinct families that incise the phosphodiester backbone 5′ to the lesion: the bacterial endonuclease IV (Nfo) family and the exonuclease III (Xth) family, which includes Xth in bacteria and

* This work was supported, in whole or in part, by National Institutes of Health (NIH), NCI, Grant P01 CA92584 and NIH, NIGMS, Grants GM046312 and CA053791 (for work on APE1 and Nfo). Work on APE1 and Nfo was also supported by National Science Foundation Career Award MCB-1149521. The Berkeley Center for Structural Biology is supported in part by NIH, NIGMS, and the Howard Hughes Medical Institute none of the authors are hhmi. The Advanced Light Source is supported under Department of Energy Contract DE-AC02-05CH11231. The Stanford Synchrotron Radiation Laboratory is supported by the Department of Energy (Office of Biological and Environmental Research), NIH (National Center for Research Resources), Biomedical Technology Program, and NIH (NIGMS).
[S] This article contains supplemental molecular dynamics models.
The atomic coordinates and structure factors (codes 4IEM and 4HNO) have been deposited in the Protein Data Bank (http://wwpdb.org/).
[1] Present address: Centre for Biosciences, Central University of Punjab, Bathinda, Punjab 151001, India.
[2] Supported in part by a Japan Society for the Promotion of Science fellowship and by the Skaggs Institute for Chemical Biology.
[3] To whom correspondence should be addressed: Life Science Division, Lawrence Berkeley National Laboratory, 1 Cyclotron Rd., Berkeley, CA 947210. Tel.: 510-486-4158; Fax: 510-486-6880; E-mail: JATainer@lbl.gov.

[4] The abbreviations used are: AP, apurinic/apyrimidinic; BER, base excision repair; MD, molecular dynamics; nt, nucleotide(s); PDB, Protein Data Bank.

AP endonuclease (APE1) in metazoan eukaryotes (10). These pivotal nucleases detect, recognize, and cleave the DNA phosphodiester backbone 5′ of AP sites to create a free 3′-OH end for repair synthesis by a DNA polymerase. The AP endonucleases also act as 3′ → 5′ exonucleases and catalyze nucleotide incision repair of particular oxidized bases (11–16). These two prototypic families mediate the same activities, but their structural folds and metal dependence are different. In initial studies of Nfo, it was differentiated from Xth by its resistance to EDTA (17, 18). The Xth family has a two-layered β-sheet core flanked by helices and is Mg^{2+}-dependent (19). In contrast, Nfo has a TIM β barrel core, surrounded by helices. It has three metal ions, either three Zn^{2+} or two Zn^{2+} and one Mn^{2+} (20). In general, understanding of distinct metal ion binding and activities, even in microbial systems, has lagged far behind genome sequencing, and an increased knowledge of structure-function relationships is fundamental to more accurate metal ion prediction for responses to stress and DNA damage (21–25). Nfo is unusual among endonucleases in that it uses Zn^{2+} ions and in that it uses three metals in its catalytic mechanism (26, 27). Three-metal mechanisms have also been proposed for *E. coli* RV, RNase H, and microbial FEN1 (28–30), but in Nfo, all three metals occupy the active site at the same time. Recent biochemical, structural, and molecular dynamics (MD) studies have defined the individual roles of each Zn^{2+}: Zn1, Zn2, and Zn3 (Fig. 1) (20, 27, 31). The initial AP site is flipped into the active site and is bound by Zn1 and Zn3. The attacking water is deprotonated by Glu-261, the one side chain directly involved in the catalytic mechanism. The resulting hydroxide ion is electrostatically stabilized by Zn1 and Zn2. All three Zn^{2+} ions stabilize the pentacoordinated transition state. At the end, Zn3 moves to coordinate the phosphate oxygen (OP′) and help stabilize the developing negative charge of the leaving group. Interestingly, crystallographic and biochemical studies suggest that the Zn3 position may actually be occupied by Mn^{2+} in *Escherichia coli*, suggesting further study.

Human APE1 (also called HAP1 and REF1) consists of a core nuclease domain that is conserved with *E. coli* Xth and a 61-residue N-terminal domain that is not conserved in bacterial proteins (32, 33). Crystal structures have shown that APE1 binds to both major and minor grooves of the DNA and flips out the abasic deoxyribose phosphate (34–37). In the original report of an APE1-DNA complex, we proposed a mechanism where Asp-210 activates the attacking water (35). The phosphate intermediate is stabilized by the Mg^{2+} ion and contacts with His-309, Asn-174, and Asn-212. Protonation of the 3′-ribose oxygen leaving group is through water in the first hydration shell of the Mg^{2+} (35), yet several subsequent papers with studies of active site mutants have proposed alternative enzyme mechanisms (38–43). These experiments were done on different mutants in different laboratories using different techniques, so no clear consensus has been reached. Even the number of metal sites participating in catalysis is in question (44), which has hampered progress.

To help resolve these questions, we solved, analyzed, and compared new crystal structures of APE1 and Nfo. A 2.4 Å resolution crystal of wild type (WT) human APE1 in a product complex with Mg^{2+} revealed a Mg^{2+}-water cluster in the active site. We determined an extremely high resolution (0.92 Å) crystallographic structure for *Thermotoga maritima* Nfo with bound metal ions. Prompted by a common substrate, we superimposed tertiary structures of APE1 and Nfo and surprisingly observed that the scissile bond can be superimposed despite differences in protein fold, metal type, and number of metals. In fact, APE1 active site residues overlay onto metal positions in Nfo. Importantly, the geometric restraints implied by the Nfo superposition are consistent with only one of multiple proposed mechanisms. Our combined structural, biochemical, and computational analyses thus help to resolve mechanistic questions and support a unified excision geometry and mechanism for the two prototypic AP endonucleases despite their structural differences.

EXPERIMENTAL PROCEDURES

Expression and Purification of APE1 and Nfo Proteins—*E. coli* Nfo, *T. maritima* Nfo, and APE1 were expressed in *E. coli* and purified as described previously (27, 35, 45–47).

APE1 Crystallization and Data Analysis—WT APE1 (12 mg/ml) was incubated with 11-mer double-stranded DNA at a molar ratio of 1:1.2 for 10 min. The DNA contained a central tetrahydrofuran on one strand as described previously (35) and was purchased from Midland Inc. The protein and DNA were mixed 1:1 with 50 mM MES, pH 6.0, 200 mM $LiSO_4$, and 25% Polyethylene glycol monomethyl ether 2,000. Crystallographic data were collected at Advanced Light Source beamline 5.0.1. Diffraction was observed to 2.1 Å, but resolution was truncated to 2.4 Å resolution due to high anisotropy and overlaps. Phases were determined by molecular replacement. Refinement was performed by CNS (48) and later by PHENIX (49). NCS restraints were combined with TLS during refinement in PHENIX. There were four molecules in the asymmetric unit. The A and C chains had the most well defined electron density, with both having *B* factor averages for all protein atoms of 42 $Å^2$. B and D chains had significantly worse density, with average *B* factors of 73 and 58 $Å^2$, respectively. The N terminus (residues 1–40) was evidently flexible because it lacked unambiguous electron density. Clear octahedral geometry for the Mg^{2+} and coordinated waters were observable in the electron density for A, C, and D. Three other Mg^{2+} sites based on coordination geometry and distances were assigned in density near A and C chains. However, coordination was to waters and to two bases in the DNA, and these other Mg^{2+} ions are unlikely to affect the catalytic mechanism. The PDB code for APE1-product complex is 4IEM.

Nfo Crystallization and Data Analysis—*T. maritima* Nfo (10 mg/ml) was crystallized in hanging drops mixed 1:1 with 100 mM Tris-HCl, pH 9.0, 4 mM DTT, 1.5% saturated $MgSO_4$, 16% ethylene glycol, 20% Polyethylene glycol monomethyl ether 2,000. Crystals were frozen with 25% ethylene glycol. Crystallographic data were collected at Stanford Synchrotron Radiation Laboratory beamline 9-1. Diffraction data were collected to 0.92 Å resolution. Refinement was consistent with a mixture of Zn^{2+} and Mn^{2+} at metal sites 2 and 3. Tests to identify manganese in the active site were not attempted at the time because occupancy of manganese was unexpected. Alternate metals could not be assigned the same number, and thus the metals

have been renumbered consecutively. Phases were determined by molecular replacement using *E. coli* Nfo (PDB code 1QTW) as a search model with the program AMORE (50) and then refined using an improved model and the program EPMR (51) with resolution limits of 8 to 4.5 Å. The solution had an R_{factor} of 0.317 and correlation coefficient (CC) of 0.725 as compared with the next solution, with an R_{factor} of 0.52 and correlation coefficient of 0.241. Refinement was performed initially with CNS (48) and later with PHENIX (49). The PDB code for the *T. maritima* Nfo is 4HNO.

Single-turnover Kinetics—Specific endonuclease activity of APE1 WT and various APE1 mutants was analyzed by single-turnover kinetics under conditions of excess enzyme and limiting substrate, a 52-nt tetrahydrofuran-containing oligonucleotide duplex (position 30 nt) (52–54). The reaction mixture (100 μl) contained 10 nM duplex oligonucleotide containing THF and 100 nM APE1. The ^{32}P-labeled oligonucleotide was diluted with unlabeled oligonucleotide to maximize the detection range. The reaction was performed at 10 °C under final buffer conditions of 50 mM Tris-HCl, pH 8.0, 50 mM KCl, and 2 mM $MgCl_2$. The reaction was initiated by adding enzyme to the reaction mixture, and 10-μl aliquots were removed at 10 s, 20 s, 30 s, 1 min, 2 min, 5 min, 10 min, 30 min, and 60 min into an equal volume of 90% formamide denaturating loading dye containing 50 mM EDTA. The samples were heat-denatured at 94 °C for 3 min. Product (30 nt) was separated from substrate (52 nt) by 20% acrylamide, 7 M urea gel. The radioactivity in these bands was quantitated in a PhosphorImager (Molecular Dynamics) using ImageQuant software.

MD of APE1 and Mutants—Models for the reactant APE1-abasic DNA complex and select mutants (E96A, D210N, N212A, H309A, H309N, and Y171F) were based on the APE1-product structure reported here and set up for classical MD using the AMBER PARM99SB force field with modified nucleic acid parameters (BSC0) (55, 56) and TIP3P solvent (57). Na^+ and Cl^- ions were used for charge neutralization and to achieve a salt concentration of 0.1 M. The protonation states for histidine residues were determined by the WHATIF server. The catalytically important His-309 residue was set as protonated. After minimization (10,000 steps) and equilibration (4-ns dynamics with gradual scaling of positional restraints), we carried out fully unconstrained production runs for WT APE1 for 15 ns. The mutant simulation trajectories were of the same length and employed the same simulation protocol as the WT APE1 except that the mutated residue was allowed to move freely and equilibrate before releasing restraints on the other active site residues. All simulations were performed in the isothermal isobaric ensemble (NPT) at 1 atm and 300 K with the program NAMD 2.8 (58). An integration time step was used under a multiple time stepping scheme. The bonded and short range interactions were calculated every third step. A short range cut-off of 10 Å was used for the short range non-bonded interactions with a switching function at 8.5 Å. The long range electrostatic interactions were treated with a smooth particle mesh Ewald method (58). The r-RESPA multiple time step method (59) was adopted with a 2-fs time step for bonded interactions, 2 fs for short range non-bonded interactions, and 4 fs for long range electrostatic interactions. We used 2-fs time steps, keeping all bonds between hydrogen and heavy atoms constrained. We visualized trajectories and computed average properties with VMD (60). Structure figures were produced using PyMOL (Schrödinger, LLC, New York) and VMD (60).

RESULTS

Crystal Structure of Human WT APE1 Bound to DNA—We crystallized full-length protein with Mg^{2+} and dsDNA containing a tetrahydrofuran. The structure was determined to 2.4 Å with an R_{factor} and R_{free} of 0.25 and 0.19, respectively (Table 1). This product structure is the highest resolution APE1-DNA complex known and a significant improvement compared with the published 3.0 Å Mn^{2+}-product complex (35). As before, there is only one metal ion observed in the active site in the asymmetric unit. The Mg^{2+} ion was identified by its coordination geometry and its distance to coordinating atoms (Fig. 1) (61).

In the three well defined active sites, only one residue, Glu-96, directly coordinates the Mg^{2+} ion. Mutation of Glu-96 reduces endonucleolytic activity 600-fold (39, 62). The 3′-ribose oxygen and the phosphate from the DNA and waters complete the tetrahedral coordination. Three waters completed the coordination. Asn-68, Asp-70, and Asp-308 coordinate the waters in the magnesium-water cluster. Mutation of these residues reduces endonucleolytic activity: Asn-68, 200-fold (36); Asp-308, 5-fold (63, 64); and Asp-70, 25-fold (39). Asp-70 is particularly intriguing because mutation enhances 3′-phosphodiesterase activity but reduces AP endonuclease activity (65). For both activities, maximum activity requires a higher Mg^{2+} concentration, consistent with a role of Asp-70 in helping to coordinate the Mg^{2+} ion through the water. Other active site waters act in indirect DNA interactions; *e.g.* Lys-98 has a water-mediated interaction with the nucleotide adjacent to the 3′-ribose oxygen. The position of the APE1 Mg^{2+} ion, between the 5′-phosphate and the 3′-hydroxyl, is on the other side of the phosphate compared with many one-metal nucleases (66).

Ultrahigh Resolution Crystal Structure of T. maritima Nfo—To obtain a greater understanding of the multiple-metal ion Nfo catalytic mechanism in comparison with the single-metal ion seen in our APE1 structures, we crystallized a hyperthermophilic ortholog from *T. maritima*. The optimal growth of this thermophile is ~80 °C (67). *T. maritima* Nfo has 33% identity with the *E. coli* enzyme, suggesting overall similarity. The protein structure was solved to 0.92 Å with an R_{factor} and R_{free} of 0.12 and 0.14, respectively (Fig. 1 and Table 1). During our study, a structure of *T. maritima* Nfo with Zn^{2+} and/or Cd^{2+} at a lower resolution, 2.3 Å, was reported (68).

As in *E. coli* Nfo, we found three metals in the active site, with a root mean square deviation of 0.2 Å from *E. coli* Nfo positions (20, 27). Previously, Mn^{2+} had been found in the Zn3 ion position in *E. coli* Nfo (27). The coordination is also more octahedral in geometry, and Nfo with Mn^{2+} is more active than with only Zn^{2+}. In our 0.92 Å structure, we could not unambiguously assign the metal 2 and 3 positions as Zn^{2+} and Mn^{2+} because the metal-ligand distances and the geometry were not definitive (61). However during refinement, we did observe negative $F_o - F_c$ difference density when Zn^{2+} was in metal 2 or 3 position and positive $F_o - F_c$ when Mn^{2+} was in those posi-

TABLE 1

X-ray diffraction data collection and refinement statistics for APE1-product DNA complex and Nfo protein

Numbers in parentheses are from the high resolution shell.

	APE1 (PDB 4IEM)	Nfo (PDB 4HNO)
DNA	Tetrahydrofuran product	
Species	*Homo sapiens*	*T. maritima*
Synchrotron	Advanced Light Source	Stanford Synchrotron Radiation Laboratory
Data collection		
Space group	$P2_1$	$P6_1$
Cell dimensions		
a, *b*, *c* (Å)	104.6, 74.1, 112.1	123.370, 123.370, 35.395
α, β, γ (degrees)	90.0, 112.0, 90.0	90.0, 90.0, 120.0
Resolution (Å)	30–2.4 Å (2.48–2.40)	30–0.92 (0.95–0.92)
R_{sym} [a]	0.064 (0.402)	0.053
$I/\sigma(I)$	11.85 (4.7)	26.5 (2.6)
Completeness (%)	90.1 (87.7)	95.9
Redundancy	3.1 (3.2)	2.84 (2.48)
Wilson *B* factor	42.2	10.2
Refinement		
Reflections (min $F/\sigma F$)	56727 (1.34)	204917 (1.34)
R_{cryst} (%) [b]	0.187	0.1248
R_{free} (%) [c]	0.250	0.1390
Molecules/asymmetric unit	4 protein, 4 dsDNA	1
No. of atoms	20,539	5274
Protein/DNA atoms	10,530	4780
Metal atoms	7 Mg^{2+}	Zn^{2+}, 2 Zn^{2+}/Mn^{2+}, Mg^{2+}
Other non-water solvent	9	61
Water atoms	272	427
B factors		
Protein/DNA	50.0	16.4
Metals	51.0	10.9
Other non-water solvent	66.1	19.7
Water	42.4	26.5
Root mean square deviations		
Bond length (Å)	0.004	0.017
Bond angles (degrees)	0.92	1.311
Ramachandran favored (%)	96	98.3
Ramachandran allowed (%)	3.7	1.7
Ramachandran outliers (%)	0.3	0

[a] R_{sym}, the unweighted *R* value on *I* between symmetry mates.
[b] $R_{cryst} = \Sigma_{hkl}||F_o(hkl)| - |F_c(hkl)||/\Sigma_{hkl}|F_o(hkl)|$.
[c] R_{free}, the cross-validation R_{factor} for 5% of reflections against which the model was not refined.

tions, suggesting either low occupancy of Zn^{2+} or a mixture of Mn^{2+} and Zn^{2+}. In the Cd^{2+} *T. maritima* Nfo structure, it was those two positions that were occupied by Cd^{2+} (68). Refinement with both Mn^{2+} and Zn^{2+} resulted in the lowest R_{factor} values and smallest difference between R_{work} and R_{free}, as compared with other refinement scenarios.

The catalytic Glu-261 and residues coordinating the three Zn^{2+} ions were absolutely conserved with *E. coli* Nfo. There was one residue different in the active site pocket. Ala-30 in *E. coli* Nfo is replaced with Gln-30 in *T. maritima* Nfo. *T. maritima* Nfo Gln-30 appeared to exclude two water molecules. We postulate that this substitution is important for *T. maritima* Nfo to have optimal endonucleolytic catalysis at 80 °C. To test this hypothesis, we compared the sequences from thermophilic and mesophic Nfo orthologs (Fig. 2). Although residue 30 was either alanine or glutamine in mesophilic Nfo, only glutamine was found at this position in thermophilic Nfo.

Superimposition of APE1 and Nfo Active Site Structures—The mechanism for Nfo has been comprehensively studied biochemically, structurally, and computationally by MD (27, 31). To better understand APE1, we compared the APE1 and Nfo structures. Examination of the DNA binding grooves in terms of the local accessibility and for fractal dimension supported the overall similarity of the active sites (70, 71) (Fig. 3). A shallow groove near the active site sterically imposes specificity for DNA lacking a bulky base. Notably, there is a significant pocket next to the active site that is present in both Nfo and APE1. We postulated that this pocket may allow the nucleotide incision repair activity and the requisite space for binding a base, albeit a non-canonical base, but simple modeling with a nucleotide incision repair substrate, an α-anomeric adenosine, did not position the base in that pocket (72). Perhaps this pocket has convergently evolved for a yet unrecognized functionality.

Because Nfo and APE1 are structurally dissimilar, we superimposed the tetrahydrofuran moiety of our 2.4 Å APE1-Mg^{2+}-product complex with that from the reported *E. coli* structure of Nfo-Zn^{2+}-product complex (PDB code 1QUM) (20). A superposition based on only the tetrahydrofuran moiety in the DNA oriented the respective scissile 5′-phosphates and 3′-ribose oxygen atoms to overlay on top of each other, supporting the hypothesis that the two enzymes have a similar mechanism (Fig. 4*A*). The root mean square deviation of the tetrahydrofuran atoms was 0.28 Å. The phosphates and ribose oxygens were 0.1 and 0.9 Å apart, respectively.

To better view any catalytic similarity of the active sites, we superimposed the scissile phosphates and ribose oxygens (Fig. 4, *B* and *C*). Because *E. coli* Nfo has three metal atoms with distinct catalytic roles (31), we were interested in which metal atom geometrically matched the Mg^{2+} atom in APE1. Superimposing the scissile phosphate and the 3′-ribose oxygens from the two structures, the Zn^{2+} atoms fall in three quadrants around the phosphate, with the Mg^{2+} in the fourth quadrant

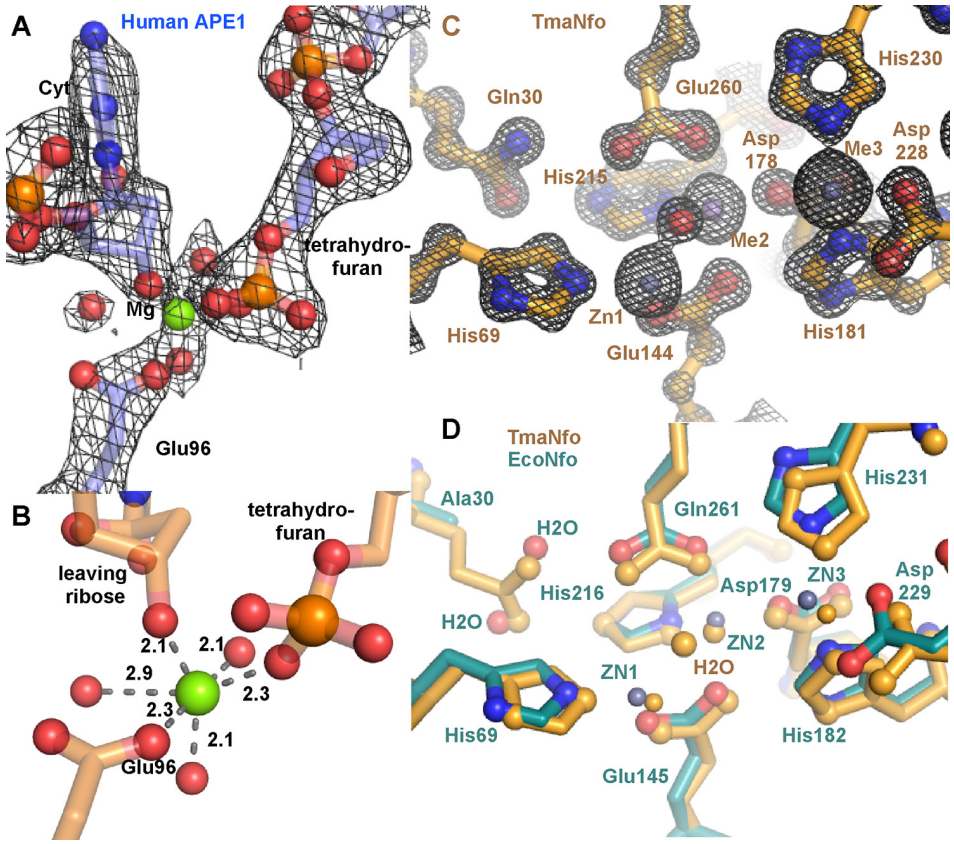

FIGURE 1. **Crystallographic structures of human APE1 and *T. maritima* Nfo showing active site details.** *A*, the 2.4 Å structure of an APE1-product complex reveals a Mg^{2+}-water cluster in the active site. Waters (*red spheres*) are shown with electron density from a PHENIX kicked map (1 σ, *blue*). *B*, simplified view of APE1 magnesium-water cluster shows tetrahedral geometry. *C*, the *T. maritima* Nfo active site structure, determined at 0.92 Å resolution. Electron density from a PHENIX kicked map (2.3 σ) is shown in *blue*. Mg^{2+} and Mn^{2+}/Zn^{2+} atoms are shown as *purple* and *dark blue spheres*. A coordinated water is shown as a *red sphere*. *D*, the superimposition of the active sites from *T. maritima* Nfo and *E. coli* Nfo reveals a single difference in the active site. Ala-30 and two waters in *E. coli* Nfo are replaced with Gln and may account for greater thermostability. These residues are next to Glu-161 (*E. coli*), which is postulated to activate the attacking water.

```
Eco 24- IDATAFALFTKN -35 mesophilic
Bth 24- IGANAFALFTKN -35 mesophilic
Tma 24- IGGNSFQIFPHN -35 thermophilic
Aae 24- IGAEVFQFFLRS -35 thermophilic
Bsu 26- YGANTFMIYTGA -37 mesophilic
Tth 26- LGLTAFQIFAKS -37 thermophilic
```

FIGURE 2. **Alignment of Nfo sequences shows that thermophilic Nfo has substituted Gln for Ala in the active site.** The region around Ala-30 in *E. coli* (*Eco*) is shown, aligned with *Bacteroides thetaiotaomicron* (*Bth*), *T. maritima* (*Tma*), *Aquifex aeolicus* (*Aae*), mesophilic *Bacillus subtilis* (*Bsu*), and *Thermus thermophilus* (*Tth*), respectively.

(Fig. 4*C*). Surprisingly, no one Zn^{2+} ion overlaid the Mg^{2+} ion. Notably, one Zn^{2+} atom (Zn1) is ~1.3 Å from the imidizole moiety of His-309 in APE1. Mutation of His-309 reduces APE1 activity over 30,000-fold (73). Another Zn^{2+} atom (Zn2) is located in between the side chains of Asn-212 and Asp-210. Zn2 also localizes ~1 Å from a second Mg^{2+} site proposed for APE1 (44). The side chain of Asn-212 (APE1) is positioned similarly to Asp-261, which directly coordinates the attacking water in Nfo. Notably, the N212A APE1 mutant lacked detectable AP endonuclease activity (74).

The third Zn^{2+} atom (Zn3) in Nfo is positioned close to APE1 Tyr-171. Zn3 is postulated to act in stabilizing the pentacoordinate intermediate. Mutation of APE1 Tyr-171 reduces AP catalytic activity more than 25,000-fold (42). Notably, because Zn3 is in a mirror position to the Mg^{2+} relative to the axis of the reaction, replacement of Zn3 with Mn^{2+} increases Nfo activity (27). No side chains from Nfo overlay in this metal position.

The one protein residue that contributes to the catalytic reaction in Nfo, Glu-261, superimposes to lie close to Asn-212 in APE1. Two Nfo residues that coordinated zinc atoms, Glu-145 and His-109, were 0.8 and 1.5 Å from Asp-210 and His-309 positions in APE1, respectively, the latter raising the possibility of the moving metal ion site. However, the measured pK_a of over 8 for His-309 is inconsistent with the need for a non-protonated imidizole necessary for metal ion coordination (75). His-109 in Nfo is not in a His-Asp pair, as is His-309 in APE1, which has Asp-308 on one side and Asp-283 on the other.

The superposition of the DNA substrates and overlay with Nfo catalytic metals highlighted the significance of four APE1 residues, Asp-210, Asn-212, His-309, and Tyr-171. From this structural comparison, it appears that APE1 residues may substitute catalytically for Nfo metals, suggesting that mutational and computation testing was merited.

Single Turnover Kinetics on Active Site Mutants—To better compare the implicated catalytic residues that have been mutated and studied in separate studies with different methods, we did single turnover kinetic studies of single site mutations on the key catalytic residues Glu-96, Tyr-171, Asp-210, Asn-212,

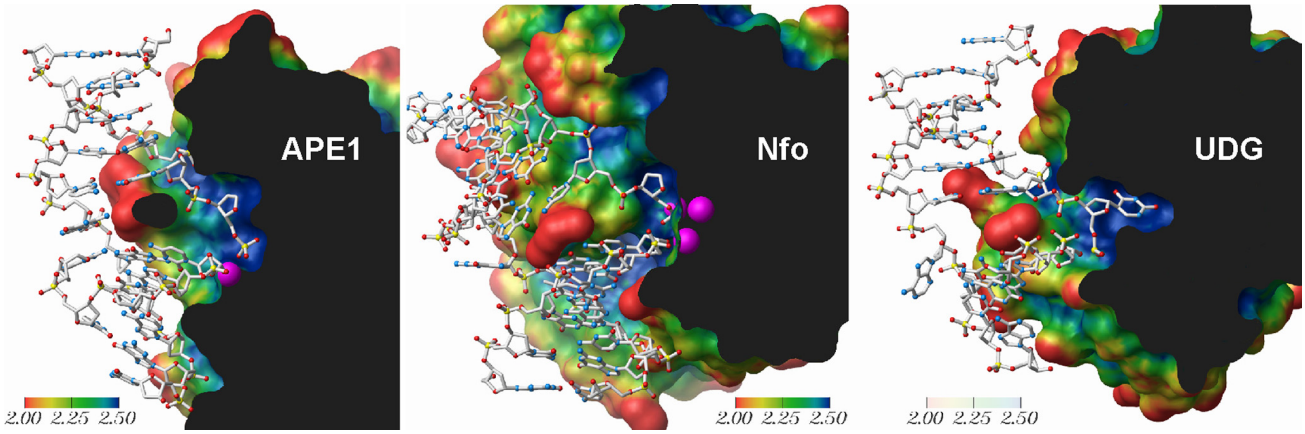

FIGURE 3. **Comparison of the fractal dimension in the DNA binding grooves of Nfo-product (PDB entry 1QUM), APE1-product (PDB entry 4IEM), and UDG (PDB entry 1EMH) highlights the shallow pockets of the AP endonucleases.** Each protein's molecular surface (calculated using MS/MS with a 1.4-Å probe sphere) is *colored* by its local atomic fractal density (70). The density is calculated using Surfractal with a 1.0–10.0 Å radius range (71). This Hausdorff-Besicovitch dimension measures the change in packing density; 2.0 indicates a flat surface, and 3.0 indicates a fully packed volume. Intermediate values identify concave grooves and pockets. This figure was created in AVS (AudioVisualSystemsInc).

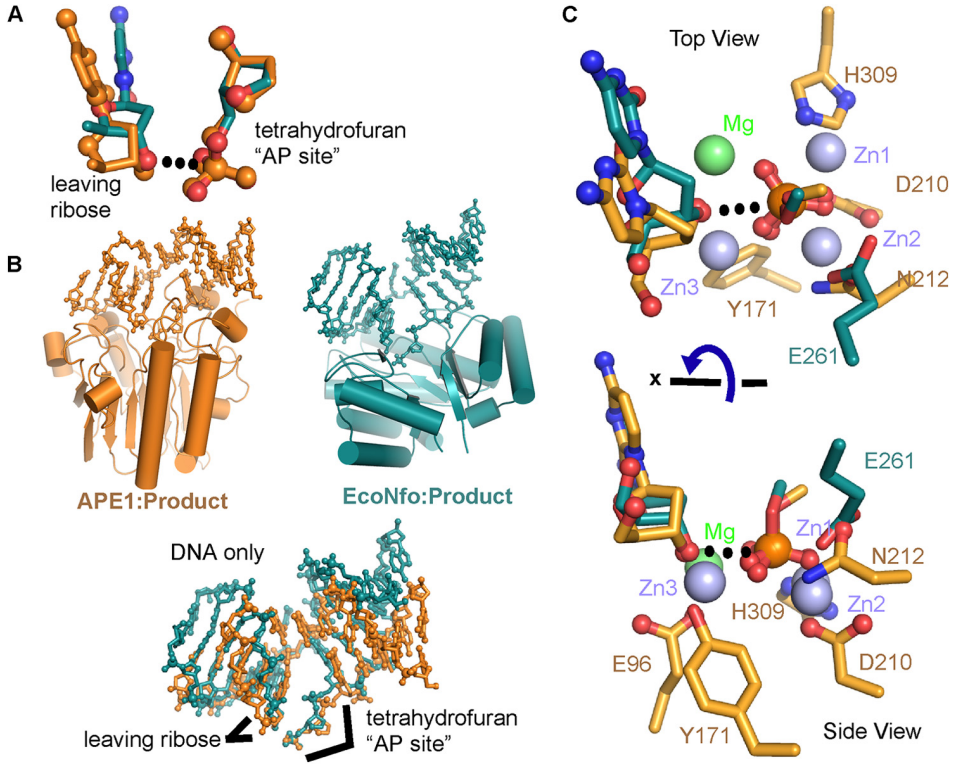

FIGURE 4. **Structural superimposition of APE1-product DNA (PDB entry 4IEM) and Nfo-product DNA (PDB entry 1QUM) based on the tetrahydrofuran moiety reveals geometric similarity.** *A*, superimposition based on the tetrahydrofuran moiety shows how similarly the tetrahydrofuran is deformed in the APE1 and Nfo structures and the close placement of the 3′-ribose oxygens. *B*, superimposition based on the scissile phosphate and the 3′-ribose oxygen shows how structurally similar the DNA products are, in contrast to the lack of conservation in tertiary structure of the proteins. *C*, close-up views of the active site showing the relative positioning of the scissile phosphate of the tetrahydrofuran and the 3′-ribose oxygen to the Mg in APE1 and the three zinc atoms in Nfo. The active site residues confirm of APE1 are shown relative to the Zn^{2+} atoms in Nfo.

and His-309 (Fig. 5). Interestingly, we found that mutation of Glu-96, the only residue that directly coordinates the Mg in the product structure, had the least effect, with activity down only by 15-fold.

In contrast, Y171F and H309N showed quite large decreases in activity of ~1200- and 2500-fold, respectively. However, Tyr-171 and His-309 were not the most important catalytic residues because their mutation was not as severe as those of Asp-210 and Asn-212. Mutants D210N and N212A were decreased 10,000- and 7000-fold in activity, respectively. Notably, Asp-210 and Asn-212 are located similarly to the two Zn^{2+} atoms (Zn1 and Zn2) found to coordinate the catalytic water in Nfo; they are positioned to coordinate a water that could make a linear attack on the phosphodiester.

To test our model computationally and provide an informed basis as to why specific mutations are reducing catalytic activity, we did MD simulations of WT and mutant APE1: E96A, Y171P, H309A, N212A, D210N, and H309N. Model coordi-

nates are part of the Supplemental Materials. In WT, we observed the catalytic water tightly hydrogen-bonded to both Asp-210 and Asn-212 with average hydrogen bond distances of 2.65 ± 0.15 and 2.83 ± 0.10 Å, respectively (Fig. 6). Interactions with these two residues position the oxygen atom of the catalytic water within 3.51 ± 0.22 Å of the scissile phosphate and orient the water for an inline attack (average O*-P-O′ angle of 162.6 ± 8.2°). Notably, the hydrogen bonding network (Fig. 6) between the catalytic water, Asp-210, Asn-212, His-309, and the abasic site phosphate is persistent throughout the MD trajectory. Indicating a less important catalytic role, mutations E96A, Y171P, and H309A did not affect the hydrogen-bonded triplet of Asp-210, Asn-212, and catalytic water, and the nucleophilic attack geometry is maintained (respective average O*-P distances of 3.52 ± 0.25, 3.51 ± 0.27, and 4.24 ± 0.69 Å). In the N212A mutant, the catalytic water is displaced from the inline position, and Asp-210 instead accepts hydrogen bonds from Asn-68 and Ala-212 (backbone). In the D210N mutant, the catalytic water does not move. However, the mutated Asn-210 side chain cannot accept a proton to activate the water. The ability of both D210N and N212A mutants to disrupt the attacking water correlates with the experimentally observed rates.

Consistent with the new APE1 crystal structure, our MD simulation of WT reveals protonated His-309 stably hydrogen-bonded to the abasic site phosphate (with average hydrogen bond distance of 2.84 ± 0.13 Å and an almost linear angle of 8.9 ± 4.7°). Experimentally, mutating His-309 has a large effect on the catalytic rate. We attribute this to electrostatic polarization and charge transfer from the positively charged His-309, which helps stabilize the developing negative charge on the phosphate moiety in the transition state. The H309N and H309A mutants would be much less effective in this role. Both mutants in MD are shown to create a water-filled cavity due to the smaller size of the Ala/Asn side chain compared with histidine. Although hydrogen bonding to the equatorial oxygen of the phosphate from nearby water molecules is still possible, neutral water molecules do not stabilize the transition state either electrostatically or through charge transfer.

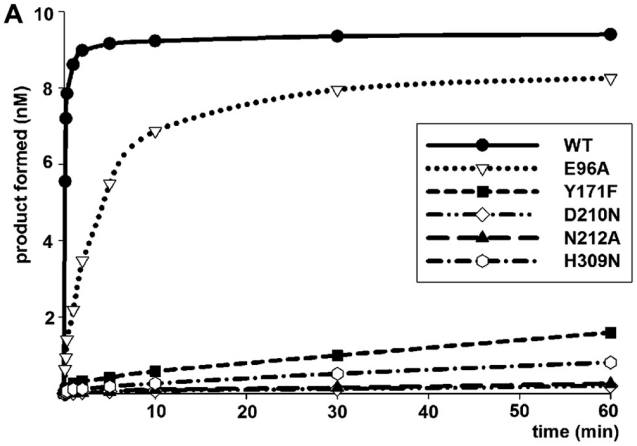

B

APE1 (WT and mutants)	Rate Constant for AP site cleavage [nmol/min]	Relative Activity
Wild type	33.3±3.281	1000±98.54
E96A	2.19±0.338	65.765±10.170
Y171F	0.0265±0.0065	0.796±0.197
D210N	0.0032±0.0018	0.097±0.055
N212A	0.0043±0.0013	0.129±0.039
H309N	0.0135±0.0042	0.407±0.128

FIGURE 5. **Single turnover kinetics of WT and APE1 mutants shows the relative importance of Asp-210 and Asn-212.** *A*, kinetics of product formation of three independent experiments for each enzyme at 10 °C. *B*, rate constants of AP site cleavage (nmol of product formation/min) at 10 °C. 52-nt THF-containing oligonucleotide duplex (10 nM) substrate and APE1 (100 nM) were used.

DISCUSSION

The value of superimposing structurally homologous proteins to understand catalytic mechanisms is well appreciated. However, it is not as intuitive to superimpose proteins that have no structural homology and that furthermore have clearly distinct metal dependences in their catalytic mechanism. Nevertheless, for APE1 and Nfo, there was surprising agreement in positions of the tetrahydrofuran and leaving 3′-ribose oxygen as well as residues and metals important for the catalytic function. The case of the evolutionary convergent catalytic triad in

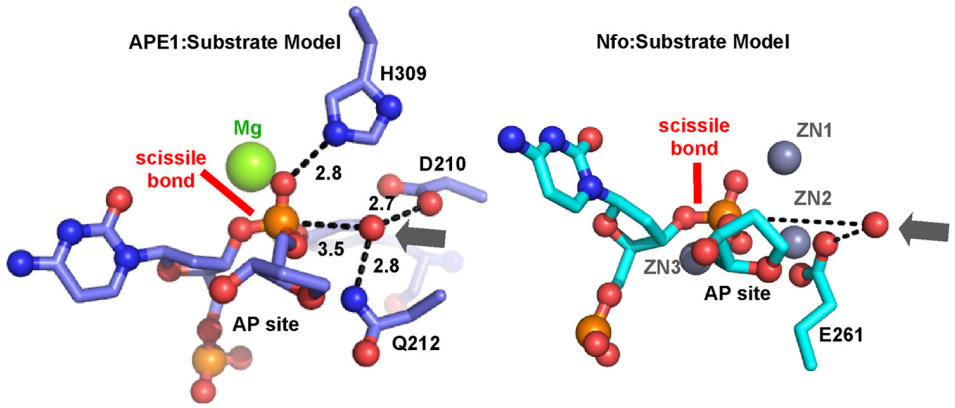

FIGURE 6. **Catalytic mechanism for APE1 and Nfo.** *A*, MD simulation of WT APE1-substrate DNA identified a persistent hydrogen bonding network, involving a water; residues His-309, Tyr-171, Asp-210, and Asn-212; and the abasic site phosphate. A snapshot from the MD trajectory shows the positions of the active site residues; hydrogen bonds (*black dotted lines*) and the nucleophilic attack direction (*gray arrow*) are shown; all distances are in Å. Tyr-171 is *below* but not labeled. *B*, model of Nfo-substrate, built from the substrate complex with E261Q (PDB entry 2NQJ) and with Glu-261 overlaid from the WT model (PDB entry 1qum).

serine proteases is analogous, except the proteins have converged on similar side chain chemistry.

For their biological functions, both APE1 and Nfo must recognize an AP site, and both flip the backbone at the AP site into a small pocket as a means of eliminating normal nucleotides with bases (10). For other DNA damage binding proteins, such as the alkylated guanine binding protein ATL, the adenine-guanine mispair glycosylase MutY, and the uracil DNA glycosylase, as well as structure-specific nucleases, such as the FEN1 superfamily and Mre11, specificity is provided by flipping of nucleotides and placing the target phosphate bond into the active site (8, 9, 76–79). APE1 and Nfo both insert loop(s) from the minor groove side (10). Flipping the AP site ~180° into the active site pockets places the scissile phosphate into a position that is amenable for catalysis. Both endonucleases use an activated water to attack the phosphodiester bond, with an electronegative phospho-intermediate whose charge needs to be alleviated for efficient catalysis. Both endonucleases need to protonate the leaving 3′-ribose oxygen. We suggest that the requirements needed to catalyze the endonucleolytic reaction define the placement of the active site structural chemistry. It is these strict geometric requirements that made the superposition informative.

Superimpositions of APE1 and Nfo with other endonucleases that do not nucleotide-flip their substrates, such as type II restriction endonucleases, were not as informative. The bonds connecting the scissile atoms diverged in angle, and metal ions did not superimpose. Thus, the successful superposition between APE1 and Nfo is unique for the two prototypic AP endonucleases and defines them in their own class. The use of a magnesium-water cluster in APE1, clearly visible in this higher resolution structure of APE1-product, is not unprecedented. There have been several cases of magnesium-water clusters reported, among them mismatch VSR endonuclease, *Serratia* and *Ppo1* homing endonucleases, *Vibrio vulnificus* periplasmic nuclease Vvn, endonuclease V that initiates deaminated adenine repair, and UVC nuclear excision repair endonuclease (80–84), Possibly significant to their substrate specificity, APE1, Vvn, and *Serratia* homing endonuclease have been shown to be active on both RNA and DNA (85–87).

Given that the reaction and damaged DNA substrate have defined the geometry, the conservation of location of an active site residue in APE1 relative to the metals in the better structurally studied Nfo provides insight into the APE1 catalytic mechanism; it allows us to plausibly assign the function of individual residues in the mechanism. The resulting mechanism is consistent with our initial model (35) but not other proposed mechanisms (38–43). Asp-210 and Asn-212 are positioned similarly to the key catalytic metals in Nfo, and their mutation was the most severe, suggesting that they coordinate the attacking water (Fig. 6).

There have been several papers published that have suggested alternative mechanisms that would be inconsistent with the geometric restraints. Because D210H was 15-fold more active than D210A or D210N, it was suggested that Asp-210 is donating a proton to the leaving group (38, 39). Asp-210 is not close to the 3′-ribose oxygen, so it could not play this role. Histidines can activate the attacking water in nuclease mechanisms, and D210H could still activate an attacking water (40, 41). It has also been suggested that Tyr-171 in a phenolate form attacks the scissile phosphate directly or generates the hydroxyl that will cleave the scissile phosphate (42). This mechanism would be similar to topoisomerases. However, the angle of attack would not be linear with the position of the 3′-ribose oxygen. In a different mechanistic model, His-309 has been suggested to generate the attacking nucleophile (43), but the geometry is also not consistent with this model. It is more than 3.5 Å from where the attacking water would be positioned. Moreover, evidence from NMR has suggested that His-309 in the APE1-DNA complex is protonated (75, 88) and thus incapable of serving as a general base. Recently, MD studies suggested that there may be a second metal binding site B, where the Mg^{2+} coordinates with Asp-210 and Asn-212, and that the one metal moves from site B to the experimentally observed metal site A during catalysis (44, 69). Our crystallographic work with one metal in site A does not show any density in position B in our 2.4 Å electron density maps. Because this absence may be due to crystallographic conditions that prevent the B position from being occupied and taking into consideration the finding that site A was occupied, the absence in the electron density does not preclude the possibility that it exists. However, the superimposition with Nfo showed that site B was between Zn2 and the probable position of the attacking water, based on the product complex. Site B is too close (1.4 Å) to the attacking water, and its coordination with both carboxylate oxygen atoms of Asp-210 would prevent Asp-210 from taking the role of directly activating the water, as suggested from our computational work (Fig. 6). The authors also suggested that the retention of magnesium dependence in an E96Q mutant indicates that site A, coordinated by Glu-96, is not important (69). Our structure of the Mg^{2+} water cluster does not suggest that an E96Q mutation would prevent Mg^{2+} from occupying site A. Thus, our combined structural, mutational, and computation results do not support the existence of a second metal site B.

Here the determination and analysis of higher resolution APE1 and Nfo structures revealed a conserved active site structural chemistry despite major differences in metal ions and structural elements. In combination with mutational and computational analyses, the structures uncover functional equivalences and support a unified mechanism for AP site excision from DNA.

Acknowledgments—Data were collected at the Advanced Light Source and Stanford Synchrotron Radiation Laboratory crystallography beamlines. Computational resources were provided by the National Science Foundation XSEDE program (Allocation CHE110042). Numan Oezguen and Werner Braun kindly shared coordinates for the model of the moving metal site. We thank James Holton and the Phenix team, Tom Terwilliger, Pavel Afonine, Nathaniel Echols, and the staff of the SIBLYS beamline for help and suggestions.

REFERENCES

1. Lindahl, T. (1993) Instability and decay of the primary structure of DNA. *Nature* **362,** 709–715
2. Lindahl, T., and Barnes, D. E. (2000) Repair of endogenous DNA damage.

Cold Spring Harb. Symp. Quant. Biol. **65,** 127–133
3. Ciccia, A., and Elledge, S. J. (2010) The DNA damage response. Making it safe to play with knives. *Mol. Cell* **40,** 179–204
4. Huffman, J. L., Sundheim, O., and Tainer, J. A. (2005) DNA base damage recognition and removal. New twists and grooves. *Mutat. Res.* **577,** 55–76
5. Loeb, L. A. (1985) Apurinic sites as mutagenic intermediates. *Cell* **40,** 483–484
6. Sobol, R. W., Kartalou, M., Almeida, K. H., Joyce, D. F., Engelward, B. P., Horton, J. K., Prasad, R., Samson, L. D., and Wilson, S. H. (2003) Base excision repair intermediates induce p53-independent cytotoxic and genotoxic responses. *J. Biol. Chem.* **278,** 39951–39959
7. Hitomi, K., Iwai, S., and Tainer, J. A. (2007) The intricate structural chemistry of base excision repair machinery. Implications for DNA damage recognition, removal, and repair. *DNA Repair* **6,** 410–428
8. Guan, Y., Manuel, R. C., Arvai, A. S., Parikh, S. S., Mol, C. D., Miller, J. H., Lloyd, S., and Tainer, J. A. (1998) MutY catalytic core, mutant and bound adenine structures define specificity for DNA repair enzyme superfamily. *Nat. Struct. Biol.* **5,** 1058–1064
9. Slupphaug, G., Mol, C. D., Kavli, B., Arvai, A. S., Krokan, H. E., and Tainer, J. A. (1996) A nucleotide-flipping mechanism from the structure of human uracil-DNA glycosylase bound to DNA. *Nature* **384,** 87–92
10. Mol, C. D., Hosfield, D. J., and Tainer, J. A. (2000) Abasic site recognition by two apurinic/apyrimidinic endonuclease families in DNA base excision repair. The 3′ ends justify the means. *Mutat. Res.* **460,** 211–229
11. Chou, K. M., and Cheng, Y. C. (2002) An exonucleolytic activity of human apurinic/apyrimidinic endonuclease on 3′ mispaired DNA. *Nature* **415,** 655–659
12. Ishchenko, A. A., Sanz, G., Privezentzev, C. V., Maksimenko, A. V., and Saparbaev, M. (2003) Characterisation of new substrate specificities of *Escherichia coli* and *Saccharomyces cerevisiae* AP endonucleases. *Nucleic Acids Res.* **31,** 6344–6353
13. Ishchenko, A. A., Yang, X., Ramotar, D., and Saparbaev, M. (2005) The 3′ → 5′ exonuclease of Apn1 provides an alternative pathway to repair 7,8-dihydro-8-oxodeoxyguanosine in *Saccharomyces cerevisiae*. *Mol. Cell Biol.* **25,** 6380–6390
14. Ischenko, A. A., and Saparbaev, M. K. (2002) Alternative nucleotide incision repair pathway for oxidative DNA damage. *Nature* **415,** 183–187
15. Kerins, S. M., Collins, R., and McCarthy, T. V. (2003) Characterization of an endonuclease IV 3′–5′ exonuclease activity. *J. Biol. Chem.* **278,** 3048–3054
16. Demple, B., Johnson, A., and Fung, D. (1986) Exonuclease III and endonuclease IV remove 3′ blocks from DNA synthesis primers in H_2O_2-damaged *Escherichia coli*. *Proc. Natl. Acad. Sci. U.S.A.* **83,** 7731–7735
17. Cunningham, R. P., Saporito, S. M., Spitzer, S. G., and Weiss, B. (1986) Endonuclease IV (nfo) mutant of *Escherichia coli*. *J. Bacteriol.* **168,** 1120–1127
18. Levin, J. D., Johnson, A. W., and Demple, B. (1988) Homogeneous *Escherichia coli* endonuclease IV. Characterization of an enzyme that recognizes oxidative damage in DNA. *J. Biol. Chem.* **263,** 8066–8071
19. Mol, C. D., Kuo, C. F., Thayer, M. M., Cunningham, R. P., and Tainer, J. A. (1995) Structure and function of the multifunctional DNA-repair enzyme exonuclease III. *Nature* **374,** 381–386
20. Hosfield, D. J., Guan, Y., Haas, B. J., Cunningham, R. P., and Tainer, J. A. (1999) Structure of the DNA repair enzyme endonuclease IV and its DNA complex. Double-nucleotide flipping at abasic sites and three-metal-ion catalysis. *Cell* **98,** 397–408
21. Cvetkovic, A., Menon, A. L., Thorgersen, M. P., Scott, J. W., Poole, F. L., 2nd, Jenney, F. E., Jr., Lancaster, W. A., Praissman, J. L., Shanmukh, S., Vaccaro, B. J., Trauger, S. A., Kalisiak, E., Apon, J. V., Siuzdak, G., Yannone, S. M., Tainer, J. A., and Adams, M. W. (2010) Microbial metalloproteomes are largely uncharacterized. *Nature* **466,** 779–782
22. Barondeau, D. P., Kassmann, C. J., Bruns, C. K., Tainer, J. A., and Getzoff, E. D. (2004) Nickel superoxide dismutase structure and mechanism. *Biochemistry* **43,** 8038–8047
23. McMurray, C. T., and Tainer, J. A. (2003) Cancer, cadmium and genome integrity. *Nat. Genet.* **34,** 239–241
24. Hopfner, K. P., Craig, L., Moncalian, G., Zinkel, R. A., Usui, T., Owen, B. A., Karcher, A., Henderson, B., Bodmer, J. L., McMurray, C. T., Carney, J. P., Petrini, J. H., and Tainer, J. A. (2002) The Rad50 zinc-hook is a structure joining Mre11 complexes in DNA recombination and repair. *Nature* **418,** 562–566
25. Castagnetto, J. M., Hennessy, S. W., Roberts, V. A., Getzoff, E. D., Tainer, J. A., and Pique, M. E. (2002) MDB. The Metalloprotein Database and Browser at The Scripps Research Institute. *Nucleic Acids Res.* **30,** 379–382
26. Dupureur, C. M. (2008) An integrated look at metallonuclease mechanism. *Curr. Chem. Biol.* **2,** 159–173
27. Garcin, E. D., Hosfield, D. J., Desai, S. A., Haas, B. J., Björas, M., Cunningham, R. P., and Tainer, J. A. (2008) DNA apurinic-apyrimidinic site binding and excision by endonuclease IV. *Nat. Struct. Mol. Biol.* **15,** 515–522
28. Horton, N. C., Newberry, K. J., and Perona, J. J. (1998) Metal ion-mediated substrate-assisted catalysis in type II restriction endonucleases. *Proc. Natl. Acad. Sci. U.S.A.* **95,** 13489–13494
29. Ho, M. H., De Vivo, M., Dal Peraro, M., and Klein, M. L. (2010) Understanding the effect of magnesium ion concentration on the catalytic activity of ribonuclease H through computation. Does a third metal binding site modulate endonuclease catalysis? *J. Am. Chem. Soc.* **132,** 13702–13712
30. Tomlinson, C. G., Syson, K., Sengerová, B., Atack, J. M., Sayers, J. R., Swanson, L., Tainer, J. A., Williams, N. H., and Grasby, J. A. (2011) Neutralizing mutations of carboxylates that bind metal 2 in T5 flap endonuclease result in an enzyme that still requires two metal ions. *J. Biol. Chem.* **286,** 30878–30887
31. Ivanov, I., Tainer, J. A., and McCammon, J. A. (2007) Unraveling the three-metal-ion catalytic mechanism of the DNA repair enzyme endonuclease IV. *Proc. Natl. Acad. Sci. U.S.A.* **104,** 1465–1470
32. Demple, B., Herman, T., and Chen, D. S. (1991) Cloning and expression of APE, the cDNA encoding the major human apurinic endonuclease. Definition of a family of DNA repair enzymes. *Proc. Natl. Acad. Sci. U.S.A.* **88,** 11450–11454
33. Walker, L. J., Robson, C. N., Black, E., Gillespie, D., and Hickson, I. D. (1993) Identification of residues in the human DNA repair enzyme HAP1 (Ref-1) that are essential for redox regulation of Jun DNA binding. *Mol. Cell Biol.* **13,** 5370–5376
34. Gorman, M. A., Morera, S., Rothwell, D. G., de La Fortelle, E., Mol, C. D., Tainer, J. A., Hickson, I. D., and Freemont, P. S. (1997) The crystal structure of the human DNA repair endonuclease HAP1 suggests the recognition of extra-helical deoxyribose at DNA abasic sites. *EMBO J.* **16,** 6548–6558
35. Mol, C. D., Izumi, T., Mitra, S., and Tainer, J. A. (2000) DNA-bound structures and mutants reveal abasic DNA binding by APE1 and DNA repair coordination. *Nature* **403,** 451–456
36. Beernink, P. T., Segelke, B. W., Hadi, M. Z., Erzberger, J. P., Wilson, D. M., 3rd, and Rupp, B. (2001) Two divalent metal ions in the active site of a new crystal form of human apurinic/apyrimidinic endonuclease, Ape1. Implications for the catalytic mechanism. *J. Mol. Biol.* **307,** 1023–1034
37. Georgiadis, M. M., Luo, M., Gaur, R. K., Delaplane, S., Li, X., and Kelley, M. R. (2008) Evolution of the redox function in mammalian apurinic/apyrimidinic endonuclease. *Mutat. Res.* **643,** 54–63
38. Maher, R. L., and Bloom, L. B. (2007) Pre-steady-state kinetic characterization of the AP endonuclease activity of human AP endonuclease 1. *J. Biol. Chem.* **282,** 30577–30585
39. Erzberger, J. P., and Wilson, D. M., 3rd (1999) The role of Mg^{2+} and specific amino acid residues in the catalytic reaction of the major human abasic endonuclease. New insights from EDTA-resistant incision of acyclic abasic site analogs and site-directed mutagenesis. *J. Mol. Biol.* **290,** 447–457
40. Galburt, E. A., Chevalier, B., Tang, W., Jurica, M. S., Flick, K. E., Monnat, R. J., Jr., and Stoddard, B. L. (1999) A novel endonuclease mechanism directly visualized for I-PpoI. *Nat. Struct. Biol.* **6,** 1096–1099
41. Tsutakawa, S. E., Jingami, H., and Morikawa, K. (1999) Recognition of a TG mismatch. The crystal structure of very short patch repair endonuclease in complex with a DNA duplex. *Cell* **99,** 615–623
42. Mundle, S. T., Fattal, M. H., Melo, L. F., Coriolan, J. D., O'Regan, N. E., and Strauss, P. R. (2004) Novel role of tyrosine in catalysis by human AP endonuclease 1. *DNA Repair* **3,** 1447–1455
43. Mundle, S. T., Delaney, J. C., Essigmann, J. M., and Strauss, P. R. (2009)

Enzymatic mechanism of human apurinic/apyrimidinic endonuclease against a THF AP site model substrate. *Biochemistry* **48,** 19–26
44. Oezguen, N., Schein, C. H., Peddi, S. R., Power, T. D., Izumi, T., and Braun, W. (2007) A "moving metal mechanism" for substrate cleavage by the DNA repair endonuclease APE-1. *Proteins* **68,** 313–323
45. Haas, B. J., Sandigursky, M., Tainer, J. A., Franklin, W. A., and Cunningham, R. P. (1999) Purification and characterization of *Thermotoga maritima* endonuclease IV, a thermostable apurinic/apyrimidinic endonuclease and 3′-repair diesterase. *J. Bacteriol.* **181,** 2834–2839
46. Izumi, T., Malecki, J., Chaudhry, M. A., Weinfeld, M., Hill, J. H., Lee, J. C., and Mitra, S. (1999) Intragenic suppression of an active site mutation in the human apurinic/apyrimidinic endonuclease. *J. Mol. Biol.* **287,** 47–57
47. Mantha, A. K., Oezguen, N., Bhakat, K. K., Izumi, T., Braun, W., and Mitra, S. (2008) Unusual role of a cysteine residue in substrate binding and activity of human AP-endonuclease 1. *J. Mol. Biol.* **379,** 28–37
48. Brünger, A. T., Adams, P. D., Clore, G. M., DeLano, W. L., Gros, P., Grosse-Kunstleve, R. W., Jiang, J. S., Kuszewski, J., Nilges, M., Pannu, N. S., Read, R. J., Rice, L. M., Simonson, T., and Warren, G. L. (1998) Crystallography & NMR system. A new software suite for macromolecular structure determination. *Acta Crystallogr. D Biol. Crystallogr.* **54,** 905–921
49. Adams, P. D., Afonine, P. V., Bunkóczi, G., Chen, V. B., Davis, I. W., Echols, N., Headd, J. J., Hung, L. W., Kapral, G. J., Grosse-Kunstleve, R. W., McCoy, A. J., Moriarty, N. W., Oeffner, R., Read, R. J., Richardson, D. C., Richardson, J. S., Terwilliger, T. C., and Zwart, P. H. (2010) PHENIX. A comprehensive Python-based system for macromolecular structure solution. *Acta Crystallogr. D Biol. Crystallogr.* **66,** 213–221
50. Navaza, J. (1994) Amore. An automated package for molecular replacement. *Acta Crystallogr. A* **50,** 157–163
51. Kissinger, C. R., Gehlhaar, D. K., and Fogel, D. B. (1999) Rapid automated molecular replacement by evolutionary search. *Acta Crystallogr. D Biol. Crystallogr.* **55,** 484–491
52. Bicknell, R., and Waley, S. G. (1985) Single-turnover and steady-state kinetics of hydrolysis of cephalosporins by β-lactamase-I from *Bacillus cereus*. *Biochem. J.* **231,** 83–88
53. Malygin, E. G., Ovechkina, L. G., Zinoviev, V. V., Linstrem, U. M., and Reich, N. O. (2001) [DNA-(N4-cytosine)-methyltransferase from *Bacillus amyloliquefaciens*. Kinetic and substrate-binding properties[. *Mol. Biol.* **35,** 42–51
54. Leipold, M. D., Workman, H., Muller, J. G., Burrows, C. J., and David, S. S. (2003) Recognition and removal of oxidized guanines in duplex DNA by the base excision repair enzymes hOGG1, yOGG1, and yOGG2. *Biochemistry* **42,** 11373–11381
55. Hornak, V., Abel, R., Okur, A., Strockbine, B., Roitberg, A., and Simmerling, C. (2006) Comparison of multiple Amber force fields and development of improved protein backbone parameters. *Proteins* **65,** 712–725
56. Pérez, A., Marchán, I., Svozil, D., Sponer, J., Cheatham, T. E., 3rd, Laughton, C. A., and Orozco, M. (2007) Refinement of the AMBER force field for nucleic acids. Improving the description of α/γ conformers. *Biophys. J.* **92,** 3817–3829
57. Jorgensen, W. L., Chandrasekhar, J., Madura, J. D., Impey, R. W., and Klein, M. L. (1983) Comparison of simple potential functions for simulating liquid water. *J. Chem. Phys.* **79,** 926–935
58. Kale, L., Skeel, R., Bhandarkar, M., Brunner, R., Gursoy, A., Krawetz, N., Phillips, J., Shinozaki, A., Varadarajan, K., and Schulten, K. (1999) NAMD2. Greater scalability for parallel molecular dynamics. *J. Comput. Phys.* **151,** 283–312
59. Tuckerman, M., Berne, B. J., and Martyna, G. J. (1992) Reversible multiple time scale molecular dynamics. *J. Chem. Phys.* **97,** 1990–2001
60. Humphrey, W., Dalke, A., and Schulten, K. (1996) VMD. Visual molecular dynamics. *J. Mol. Graph. Model.* **14,** 33–38
61. Harding, M. M. (2001) Geometry of metal-ligand interactions in proteins. *Acta Crystallogr. D Biol. Crystallogr.* **57,** 401–411
62. Rothwell, D. G., Hang, B., Gorman, M. A., Freemont, P. S., Singer, B., and Hickson, I. D. (2000) Substitution of Asp-210 in HAP1 (APE/Ref-1) eliminates endonuclease activity but stabilises substrate binding. *Nucleic Acids Res.* **28,** 2207–2213
63. Barzilay, G., Mol, C. D., Robson, C. N., Walker, L. J., Cunningham, R. P., Tainer, J. A., and Hickson, I. D. (1995) Identification of critical active-site residues in the multifunctional human DNA repair enzyme HAP1. *Nat. Struct. Biol.* **2,** 561–568
64. Masuda, Y., Bennett, R. A., and Demple, B. (1998) Dynamics of the interaction of human apurinic endonuclease (Ape1) with its substrate and product. *J. Biol. Chem.* **273,** 30352–30359
65. Castillo-Acosta, V. M., Ruiz-Pérez, L. M., Yang, W., González-Pacanowska, D., and Vidal, A. E. (2009) Identification of a residue critical for the excision of 3′-blocking ends in apurinic/apyrimidinic endonucleases of the Xth family. *Nucleic Acids Res.* **37,** 1829–1842
66. Yang, W. (2008) An equivalent metal ion in one- and two-metal-ion catalysis. *Nat. Struct. Mol. Biol.* **15,** 1228–1231
67. Huber, R., Langworthy, T. A., Konig, H., Thomm, M., Woese, C. R., Sleytr, U. B., and Stetter, K. O. (1986) *Thermotoga maritima* Sp-Nov represents a new genus of unique extremely thermophilic eubacteria growing up to 90 °C. *Arch. Microbiol.* **144,** 324–333
68. Tomanicek, S. J., Hughes, R. C., Ng, J. D., and Coates, L. (2010) Structure of the endonuclease IV homologue from *Thermotoga maritima* in the presence of active-site divalent metal ions. *Acta Crystallogr. Sect. F Struct. Biol. Cryst. Commun.* **66,** 1003–1012
69. Oezguen, N., Mantha, A. K., Izumi, T., Schein, C. H., Mitra, S., and Braun, W. (2011) MD simulation and experimental evidence for Mg^{2+} binding at the B site in human AP endonuclease 1. *Bioinformation* **7,** 184–198
70. Sanner, M. F., Olson, A. J., and Spehner, J. C. (1996) Reduced surface. An efficient way to compute molecular surfaces. *Biopolymers* **38,** 305–320
71. Kuhn, L. A., Siani, M. A., Pique, M. E., Fisher, C. L., Getzoff, E. D., and Tainer, J. A. (1992) The interdependence of protein surface topography and bound water molecules revealed by surface accessibility and fractal density measures. *J. Mol. Biol.* **228,** 13–22
72. Aramini, J. M., Cleaver, S. H., Pon, R. T., Cunningham, R. P., and Germann, M. W. (2004) Solution structure of a DNA duplex containing an α-anomeric adenosine. Insights into substrate recognition by endonuclease IV. *J. Mol. Biol.* **338,** 77–91
73. Lucas, J. A., Masuda, Y., Bennett, R. A., Strauss, N. S., and Strauss, P. R. (1999) Single-turnover analysis of mutant human apurinic/apyrimidinic endonuclease. *Biochemistry* **38,** 4958–4964
74. Rothwell, D. G., and Hickson, I. D. (1996) Asparagine 212 is essential for abasic site recognition by the human DNA repair endonuclease HAP1. *Nucleic Acids Res.* **24,** 4217–4221
75. Lowry, D. F., Hoyt, D. W., Khazi, F. A., Bagu, J., Lindsey, A. G., and Wilson, D. M., 3rd. (2003) Investigation of the role of the histidine-aspartate pair in the human exonuclease III-like abasic endonuclease, Ape1. *J. Mol. Biol.* **329,** 311–322
76. Tubbs, J. L., Latypov, V., Kanugula, S., Butt, A., Melikishvili, M., Kraehenbuehl, R., Fleck, O., Marriott, A., Watson, A. J., Verbeek, B., McGown, G., Thorncroft, M., Santibanez-Koref, M. F., Millington, C., Arvai, A. S., Kroeger, M. D., Peterson, L. A., Williams, D. M., Fried, M. G., Margison, G. P., Pegg, A. E., and Tainer, J. A. (2009) Flipping of alkylated DNA damage bridges base and nucleotide excision repair. *Nature* **459,** 808–813
77. Tsutakawa, S. E., Classen, S., Chapados, B. R., Arvai, A. S., Finger, L. D., Guenther, G., Tomlinson, C. G., Thompson, P., Sarker, A. H., Shen, B., Cooper, P. K., Grasby, J. A., and Tainer, J. A. (2011) Human flap endonuclease structures, DNA double-base flipping, and a unified understanding of the FEN1 superfamily. *Cell* **145,** 198–211
78. Grasby, J. A., Finger, L. D., Tsutakawa, S. E., Atack, J. M., and Tainer, J. A. (2012) Unpairing and gating. Sequence-independent substrate recognition by FEN superfamily nucleases. *Trends Biochem. Sci.* **37,** 74–84
79. Williams, R. S., Moncalian, G., Williams, J. S., Yamada, Y., Limbo, O., Shin, D. S., Groocock, L. M., Cahill, D., Hitomi, C., Guenther, G., Moiani, D., Carney, J. P., Russell, P., and Tainer, J. A. (2008) Mre11 dimers coordinate DNA end bridging and nuclease processing in double-strand-break repair. *Cell* **135,** 97–109
80. Li, C. L., Hor, L. I., Chang, Z. F., Tsai, L. C., Yang, W. Z., and Yuan, H. S. (2003) DNA binding and cleavage by the periplasmic nuclease Vvn. A novel structure with a known active site. *EMBO J.* **22,** 4014–4025
81. Truglio, J. J., Rhau, B., Croteau, D. L., Wang, L., Skorvaga, M., Karakas, E., DellaVecchia, M. J., Wang, H., Van Houten, B., and Kisker, C. (2005) Structural insights into the first incision reaction during nucleotide exci-

sion repair. *EMBO J.* **24,** 885–894
82. Miller, M. D., Cai, J., and Krause, K. L. (1999) The active site of *Serratia* endonuclease contains a conserved magnesium-water cluster. *J. Mol. Biol.* **288,** 975–987
83. Dalhus, B., Arvai, A. S., Rosnes, I., Olsen, Ø. E., Backe, P. H., Alseth, I., Gao, H., Cao, W., Tainer, J. A., and Bjorås, M. (2009) Structures of endonuclease V with DNA reveal initiation of deaminated adenine repair. *Nat. Struct. Mol. Biol.* **16,** 138–143
84. Flick, K. E., Jurica, M. S., Monnat, R. J., Jr., and Stoddard, B. L. (1998) DNA binding and cleavage by the nuclear intron-encoded homing endonuclease I-PpoI. *Nature* **394,** 96–101
85. Barnes, T., Kim, W. C., Mantha, A. K., Kim, S. E., Izumi, T., Mitra, S., and Lee, C. H. (2009) Identification of Apurinic/apyrimidinic endonuclease 1 (APE1) as the endoribonuclease that cleaves c-myc mRNA. *Nucleic Acids Res.* **37,** 3946–3958
86. Wu, S. I., Lo, S. K., Shao, C. P., Tsai, H. W., and Hor, L. I. (2001) Cloning and characterization of a periplasmic nuclease of *Vibrio vulnificus* and its role in preventing uptake of foreign DNA. *Appl. Environ. Microbiol.* **67,** 82–88
87. Nestle, M., and Roberts, W. K. (1969) An extracellular nuclease from *Serratia marcescens*. II. Specificity of the enzyme. *J. Biol. Chem.* **244,** 5219–5225
88. Lipton, A. S., Heck, R. W., Primak, S., McNeill, D. R., Wilson, D. M., 3rd, and Ellis, P. D. (2008) Characterization of Mg^{2+} binding to the DNA repair protein apurinic/apyrimidic endonuclease 1 via solid-state ^{25}Mg NMR spectroscopy. *J. Am. Chem. Soc.* **130,** 9332–9341